DISKS FALLING IN TO TURBULENCE

Luis Blay Esteban
Faculty of Engineering and the Environment
University of Southampton
University Road, Southampton, SO17 1BJ
lbe1g14@soton.ac.uk

John Shrimpton
Faculty of Engineering and the Environment
University of Southampton
University Road, Southampton, SO17 1BJ
lbe1g14@soton.ac.uk

Bharath Ganapathisubramani
Faculty of Engineering and the Environment
University of Southampton
University Road, Southampton, SO17 1BJ
lbe1g14@soton.ac.uk

ABSTRACT

This paper details experimental results on the dynamics of freely falling inertial disks settling through turbulence. The three dimensional particle motion is obtained using an orthogonal arrangement of two high speed cameras, whereas turbulence is generated in a water tank using a random jet array (RJA) facility with two planes of jets facing the centre of the tank. The facility is in operation until turbulence reaches a statistically stationary state, then it is turned off and a disk is released after a given waiting time (dt). Three flow conditions corresponding to different waiting times are tested; i.e. $dt = 2$s, $dt = 10s$ and $dt = 20$s. We observe significant changes in the falling style of disks when these descent through a turbulent media when compared to the disk periodic motion in quiescent flow. Extreme events that do not occur in still fluid are reported, such as the 'slow tumbling' and 'levitating' events. Contrary to the effect observed for spherical particles, finite-size inertial disks exhibit an increase in descent velocity for turbulence velocity fluctuations smaller than the particle descent velocity in quiescent flow. We observed a consistent increase in mean descent velocity as turbulence velocity fluctuations increase. Thus, the flow condition with higher turbulence velocity fluctuations induces a severe enhancement of the particle descent velocity; and this corresponds to about 20% of the descent velocity in quiescent flow for the disk with higher dimensionless inertia.

Introduction

Multiphase flows with a dispersed solid phase are common in many everyday phenomena; ranging from natural systems, as in marine biology, to engineering applications such as hydraulics or civil engineering. Two-phase flows are an interesting topic of research since in most of these situations the carrier media is characterized by having a turbulent behaviour. Furthermore, solids can appear in a polydispersed phase with complex geometries far from being spherical, causing complex particle-fluid interactions.

The motion of free falling disks, as one of the simplest non-spherical geometries, has been extensively investigated during the last decades. Willmarth *et al.* (1964) were the first to define the regime map in the $Re - I^*$ domain, where three different falling modes were reported; i.e. 'Steady', 'Fluttering' and 'Tumbling'. The Reynolds number defined as $Re = V_z D/\nu$ and the dimensionless moment of inertia as $I^* = \pi \rho_p h / 64 \rho_f D$, where V_z is the mean descent velocity, D is the disk diameter, ν the fluid kinematic viscosity, ρ stands for density and h for disk thickness. Some years later, the experimental work of Field *et al.* (1977) found the 'Chaotic' regime and included it in the $Re - I^*$ domain, separating the 'Fluttering' and 'Tumbling' regimes. Contrary to what was previously belived, they reported that this motion was not a transient state between 'Fluttering' and 'Tumbling' but that disks under this regime showed a continuous transition from 'Fluttering' to 'Tumbling' during the fall. Recent experimental work in Zhong *et al.* (2011) established three further sub-modes all within the 'Fluttering' regime defined by Willmarth *et al.* (1964). These were reported to be almost entirely defined by the dimensionless moment of inertia and were labelled as 'Planar zig-zag', 'Transition' and 'Spiral'. Futher experimental work in Zhong *et al.* (2013) and Lee *et al.* (2013) showed that disks lying in the boundary between 'Planar zig-zag' and 'Transition' regimes can describe both types of descent during in a single realization. They also showed severe differences in the structure of the wake of the disks when describing one type of descent or another. On the other hand, numerical simulations have been also performed on the low to moderate Reynolds number parameter space, as in Auguste *et al.* (2013) and Churst *et al.* (2013). These studies identified several other three dimensional sub-modes that cannot be easily observed in the experimental environment due to the low amplitude of the lateral oscillations compared with the disk diameter.

Similarly, other irregular particles than disks have been investigated experimentally, as in Esteban *et al.* (2018, 2019), and the introduction of sharp edges or indentations have been found to trigger the transition from one falling style to another.

Despite of the extensive research on the descent of irregular particles in quiescent flow, very little is known about the motion of such particles falling through a turbulent media. Thus, the objective of this experimental study is to compare the 3−D particle trajectory of disks settling through a homogeneous turbulence with the case of quiescent flow.

Experimental setup
Facilities

The experiments were conducted in a water tank equipped with a co-planar arrangement of random jet arrays (RJA). The water tank is an open glass (bottom and walls) and steel-framed tank of dimensions $200 \times 85 \times 100\,\mathrm{cm}^3$ and the RJA are located at a distance of 165 cm from each other. The structure holding the water tank is designed so that the central region of the tank (100×90 cm) is optically accessible from the bottom. The tank was filled with tap water, of density $0.996\,\mathrm{g\ cm}^{-3}$, to a height of 80 cm. The kinematic viscosity was estimated to be $1.02 \times 10^{-6}\,\mathrm{m}^2\mathrm{s}^{-1}$ at room temperature (20^oC).

Turbulence is generated by operating the two facing planes of randomly jet arrays, in the same fashion as in Esteban *et al.* (2019). Each plane of jets contains 48 bilge pumps (Rule 24, 360 GPH) arranged in a cartesian grid of 8×6, as in figure 1. The pumps take in water radially at their base and discharge it axially via a cylindrical nozzle (1.8 cm inner diameter). Each pump acts as a synthetic jet, in the sense that they only inject momentum to the system, since the pump intake and nozzle are contained within the same volume of fluid. Each plane of bilge pumps is connected to a solid state relay rack SSR-RACK48 equipped with quad-core relays SSR-4-ODC-05. The relays are triggered by TTL signals from a Measurement Computing 96 channel digital output card (PCI-DIO96H) controlled by MATLAB. The firing algorithm we employ to force turbulence is the 'Sunbathing' algorithm originally proposed in Variano & Cowen (2008), and latter investigated in Bellani & Variano (2013), Carter *et al.* (2016) and Esteban *et al.* (2019) among others. The average amount of pumps that are employed at a given time is $\phi = 12.5\%$.

Different test cases were achieved by keeping the disk and fluid density constant but changing the disk thickness h and diameter D. All disks were made of aluminium with a density of $2.70\,\mathrm{g\ cm}^{-3}$. The disk material properties, Archimedes number Ar and dimensionless moment of inertia I^* are summarized in table 1. The Archimedes number $Ar = \sqrt{3/32}U_gD/nu$, which can be defined as a Reynolds number based on the gravitational speed $U_g = \sqrt{2(\rho_p/\rho_f - 1)gh}$, has been recently considered to be one of the true control parameters (see Auguste *et al.* (2013)) since the gravitational speed is known *a priori*. The disks used in this study were manufactured to lie in the $(Ar - I^*)$ domain corresponding to the 'Fluttering' regime first defined in Willmarth *et al.* (1964) and more precisely in the 'Planar zig-zag' sub-regime defined in Zhong *et al.* (2011). Therefore, we expect them to describe a highly planar oscillatory motion when released in quiescent flow. This will reduce the variability in the natural descent of the particle, revealing more clearly the effect of background turbulence. In all experiments, the disks were released using a mechanism that employs active suction and is capable of accommodating all disks considered here. When the suction circuit is opened the pressure difference maintaining the particle fixed vanishes and the particle begins its descent through the tank. The suction system was part of a rigid frame attached to the top of the water tank, ensuring that the particle initial conditions were the same in all realizations ($V_{t=0} = 0$, $\theta_{t=0} = 0 \pm 0.1$, with θ being the particle inclination angle).

Disk	d [mm]	t [mm]	ρ[g/cm^3]	Ar	I^*
$\sharp$1	10	0.5	2.7	393	6.11 $\times 10^{-3}$
$\sharp$2	12.5	0.5	2.7	492	5.44 $\times 10^{-3}$
$\sharp$3	15	1	2.7	835	8.52 $\times 10^{-3}$

Table 1. Main geometric and material parameters of the disks that define the Archimedes number (Ar) and the dimensionless moment of inertia (I^*).

Measurement of the body motion

The location of the disk was measured using a stereoscopic vision system consisting of two digital cameras and diffuse light source, as shown in figure 1. The cameras (JAI GO-5000M USB) were used to capture two views of the falling particle. Careful attention was paid to the camera alignment to make the two views orthogonal for the latter digital processing and trajectory reconstruction. One camera recorded the front-view of the descend while the other recorded the bottom-view of the descend through a mirror at 45^o. The cameras were synchronized and triggered using an external 5 V signal sent from an Arduino. The trajectories were recorded at 60 frames per second and this frame-rate was sufficient to resolve the translation motion during all parts of the descent. In each frame the dark particle projection is recorded onto the white background and the position of the particle center of mass was obtained by locating the geometric center of each particle projection. The image processing was performed using an in-house script developed in MATLAB, as in Esteban *et al.* (2018, 2019). The method to obtain the particle position from the grey-scale image is a threshold based method, where raw images are converted into black and white images after applying a user defined intensity threshold. For the accuracy on the particle location we rely on a stable light intensity during all parts of the trajectory. Commercial LED panels connected to a stable DC power supply were used to back illuminate the field of view. Both LED panels are mounted to cover the complete field of view of both cameras; i.e. 60×60 cm for the bottom view and 60×80 cm for the front view.

The measured trajectories were smooth, but a polynomial filter of 3^{rd} order and frame length of 5 points was used to filter out high frequency noise. Both cameras were always positioned at a relative small distance from the tank to have a good compromise between field of view and number of pixels per particle diameter. The process followed to obtain the particle center of mass did not add any uncertainty for the case of a thin disk.

A set of releases of a polylactide (PLA) sphere falling in air was performed to establish limitations on the accuracy associated with the drop mechanism as well as the measurements taken by the cameras and account for image distortion from the lens. The variance in the landing position was a measure of the uncertainty of the system, being two orders of magnitude smaller than the sphere diameter. The magnitude of the uncertainty is in accordance with similar systems found in the literature, (Heisinger *et al.*, 2014).

Methods

In all experiments, the disk was released with the same initial conditions ($V_{t=0} = 0$, $\theta_{t=0} = 0 \pm 0.1^o$). The disks were dropped from a height sufficiently large ($80\,cm$) to allow the falling regime to fully develop during the observation. This vertical path corresponds to 80, 64 and 53 disk diameters for the particles investigated. Each disk was released 50 times in quiescent flow to establish the dynamics of the motion without the influence of background turbulence.

The determination of the distance at which the particle motion is not influenced by the initial transient dynamics in quiescent flow is non-trivial. In here, the term 'saturated path' stands for the section of the trajectory for which the statistics of the motion are independent of the vertical distance z. Churst *et al.* (2013) performed simulations of an infinitely thin disks with $I^* = 3.12 \times 10^{-3}$ and $Ga = 300$ and showed that it reached a 'saturated path' at a vertical distance of $\approx 60D$ from the release point, whereas Heisinger *et al.* (2014) showed experimentally that for disks with $I^* \approx 3 \times 10^{-3}$ and $Ga \approx 4180$, the disk trajectory was 'saturated' after a distance of $7D$. Here the disks has a higher dimensionless inertia than in Heisinger *et al.* (2014), with $I^* \approx 6-8 \times 10^{-3}$ and $Re \approx 1000-2300$ (or equivalent Galileo number $Ga = 1.15-2.12 \times 10^4$) but we also observed that a vertical distance of $7D$ from the release mechanism was enough to reach a 'saturated path'. Thus, a distance of $7D$ is given to the particle to accommodate to the fall before the trajectories are analysed.

As discussed in Heisinger *et al.* (2014), the bottom of the tank influences the landing position of the particle due to hydrodynamic interactions and the particle persistent motion once it is flat on top of the glass surface. To overcome these influences we do not process the particle trajectory once it reaches a distance of $2D$ from the bottom of the tank. Thus, we save trajectory sections that goes from $7D$ from the top (corresponding to a location were the particle trajectory is at a 'saturated' state) to $2D$ from the bottom (unperturbed by the glass surface).

After the experiments in quiescent flow, each disk was released in a turbulent environment (200 realizations per case). To recreate turbulent scenarios with similar flow characteristics the water tank was actively stirred using both RJA's for a period of 5 min until the turbulence level reached a statistically stationary state. Then, all pumps were turned off simultaneously and a disk was released after a given waiting time (dt). The scenarios considered in this study are $dt = 2$, 10 and 20 s.

Figure 2 shows the turbulent kinetic energy in the facility at these points during the decay, here expressed as $q^2 = u_1^2 + 2u_2^2$, due to the symmetric character of the facility (see Esteban *et al.* (2019)). The red, orange and yellow rectangles in figure 2 represent the level of turbulent kinetic energy experienced by the disk throughout the descent at different waiting times. These colours will be used in the discussion to represent quantities at the three waiting times considered.

Results

Falling style

The three disks show a 'Planar zig-zag' descent motion with very small deviations from the idealized planar motion when release in quiescent flow, as expected from the magnitudes of the Archimedes and dimensionless moment of inertia shown in table 1. For brevity, only a sample trajectory corresponding to disk ♯2 is shown in figure 3.

On the other hand, sample particle trajectories falling under the effect of background turbulence are plotted in figure 4 to allow visual comparison with the highly periodic disk trajectory in quiescent flow (figure 3), and a few interesting events are observed for the cases presented. In figure 4 a) one can observe that the disk, strongly influenced by large turbulent structures in the flow, can describe low frequency oscillations in the $X-Y$ plane, leading to a preferen-

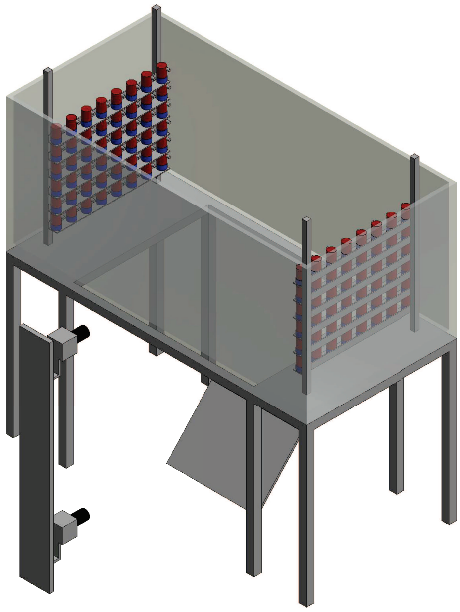

Figure 1. Sketch of the water tank equipped with a coplanar arrangement of random jet arrays (RJA). The central region of the frame allows optical access from the bottom; in here through a mirror at 45^o.

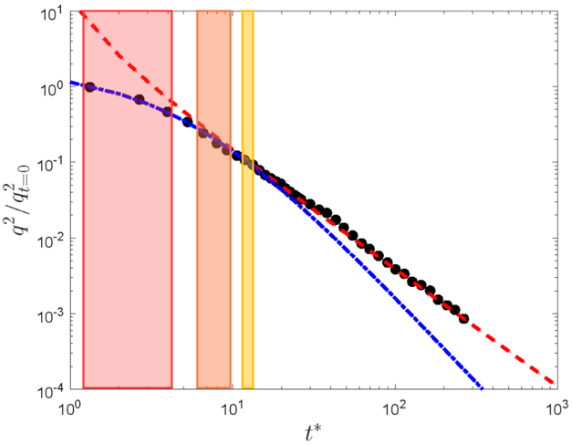

Figure 2. Time evolution of the turbulent kinetic energy during the decay; $q^2 = {u'_1}^2 + 2{u'_2}^2$. Time is made dimensionless with the eddy turnover time at the start of the decay (t_L) as $t^* = t/t_L$. The dashed-dotted line represents the near-field and the dashed line the far-field of the decay. The red, orange and yellow rectangles show the statistical turbulent kinetic energy that the disks will experience during the fall for $dt = 2$, 10, 20 s, respectively.

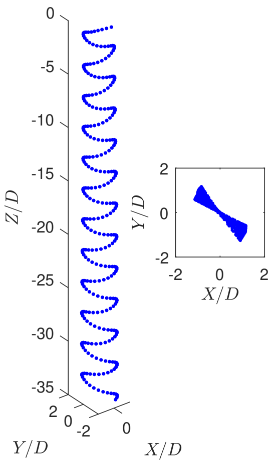

Figure 3. Reconstructed 3D trajectories and (X,Y) planar projection for disk $\sharp 2$ released in quiescent flow. The particle dispersion is normalized with the disk diameter.

tial lateral motion during sections of the descent. More precisely, we observe that the disk describes a lateral motion of about $10D$ in amplitude in one lateral direction while fluttering to latter reverse the mean lateral motion back during the second half of the descent. At the same time, one can observe in all figures very long gliding sections during the descent that increase severely the particle dispersion. Similarly, the local slope of the gliding sections (and therefore particle nutation angle θ) is considerably higher than in the case of quiescent flow. However, this does not occur after every turning section but depends on the local flow around the particle.

We believe that the long gliding sections are caused by the flow to be moving locally in the same direction as the natural motion of the particle and therefore enhancing the particle flutter. However, these long gliding events can be attenuated during the descent and be substituted by 'standard' fluttering, as in figure 4 b) for the trajectory section corresponding to $-20 < Z/D < -30$. On the other hand, we believe that trajectory sections of high nutation angle are governed by the particle-turbulence interaction during the previous turning event. Thus, when a turbulent structure destabilizes the particle at the turning point (where particle speed is smaller) it induces a higher particle nutation angle and it strongly modifies the particle local descent (until the new turning point is reached).

Mean descent velocity

The ratio between the descent velocity of the particles in quiescent conditions (defined as $\tau_p g$ for spherical particles) and the mean velocity fluctuations has been extensively used to determine the change in settling speed of inertial particles (Nielsen (1993), Good *et al.* (2012, 2014) and Byron *et al.* (2015)). In here, the gravitational velocity ($\tau_p g$) is substituted by the descent velocity in quiescent flow ($\langle V_z \rangle$) due to the difficulties associated with defining an appropriate particle relaxation time for particles with strong secondary motions. Thus, the ratio $\langle V_z \rangle / u'$, where u' stands for the r.m.s of the turbulence velocity fluctuations, is included in table 2 for each particle and flow condition tested.

For small ($D << \eta$) and heavy ($\rho_p >> \rho_f$) spherical particles, Good *et al.* (2014) found that turbulence enhances the settling of particles for particle gravitational velocities smaller than the turbulence velocity fluctuations ($\tau_p g/u' < 1$), whereas the settling is inhibited when the turbulence velocity fluctuations are smaller than the particle gravitational velocities ($\tau_p g/u' > 1$). However, the change in mean descent velocity might not follow the same trend when aspherical particles with strong secondary motion are considered.

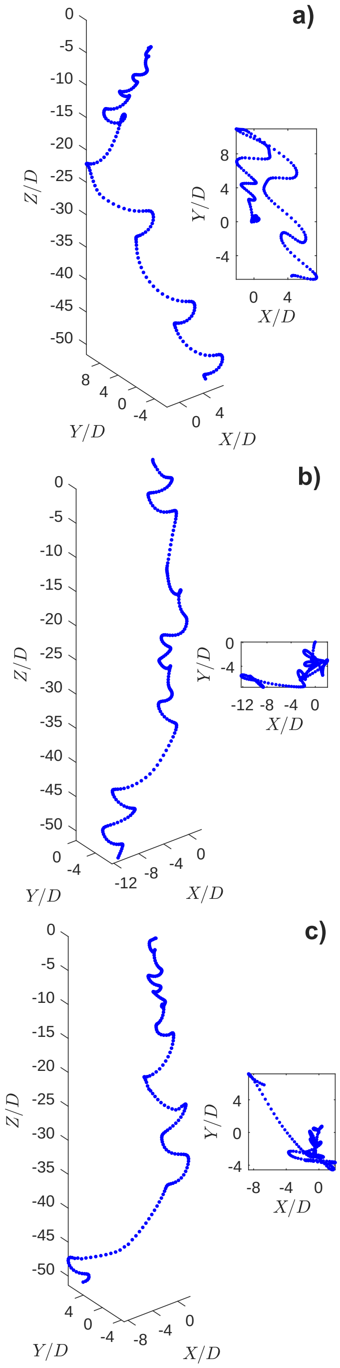

Figure 4. Reconstructed 3D trajectories and (X,Y) planar projection for disk $\sharp 1$ released after of waiting time $dt = 2$. The particle dispersion is normalized with the disk diameter.

In here, the r.m.s of the velocity fluctuations never exceeds the value of the particle descent velocity in quiescent flow and represents a velocity fluctuation of about $0.7\langle V_z \rangle$ for the shortest waiting time ($dt = 2$s). Therefore, being in the $\tau_p g/u' > 1$ scenario, particles should always fall slower

		$\langle V_{q_z}\rangle/u'$	L/D	λ/D	η/D
Disk $\sharp 1$	$dt=2$	1.50	9.1	3.6	0.016
	$dt=10$	3.17	9.42	4.2	0.093
	$dt=20$	4.25	9.9	4.9	0.155
Disk $\sharp 2$	$dt=2$	1.45	7.28	2.87	0.0128
	$dt=10$	3.07	7.54	3.34	0.0744
	$dt=20$	4.11	7.92	3.92	0.133
Disk $\sharp 3$	$dt=2$	2.50	6.06	2.39	0.011
	$dt=10$	5.27	6.28	2.78	0.062
	$dt=20$	7.07	6.6	3.26	0.111

Table 2. Values of the particle-turbulence velocity ratio ($\langle V_{q_z}\rangle/u'$) and main turbulent structures to particle diameter ratios, where L stands for the integral lengthscale, λ for the Taylor lengthscale and η for the Kolmogorov lengthscale

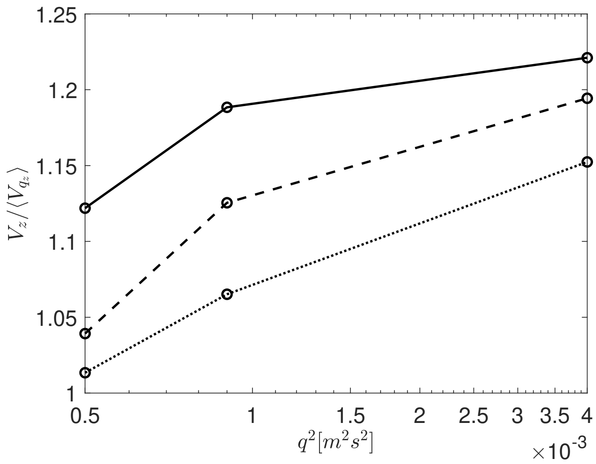

Figure 5. Evolution of the mean descent velocity of inertial disks as a function of the turbulence intensity. The descent velocity of the particles is normalized using the mean descent velocity of the particle in quiescent flow ($\langle V_{q_z}\rangle$). Dotted line stands for disk $\sharp 1$, broken line for disks $\sharp 2$ and solid line for disk $\sharp 3$.

than in quiescent flow if the trend for spherical particles is maintained.

Figure 5 shows the ratio of the mean descent velocity of the particle under turbulent conditions to the descent velocity in quiescent flow. Contrary to what one would expect, the mean descent velocity increases significantly as the turbulence intensity in the facility does so.

Figure 6 shows the data corresponding to the 200 trajectories per disk (a) Disk $\sharp 1$, b) Disk $\sharp 2$, c) Disk $\sharp 3$) and waiting time ($dt = 2$s in red, $dt = 10$s in orange and $dt = 20$s in yellow) in the form of probability density functions (PDF) of the mean descent velocity per trajectory. As expected from the results in figure 5, these figures show that as the turbulent kinetic energy increases all three disks exhibit fast descents more often than in quiescent flow. In some extreme instances, the mean descent velocity along a single trajectory can double the descent velocity of the disk in quiescent flow. However, one can also observe that the

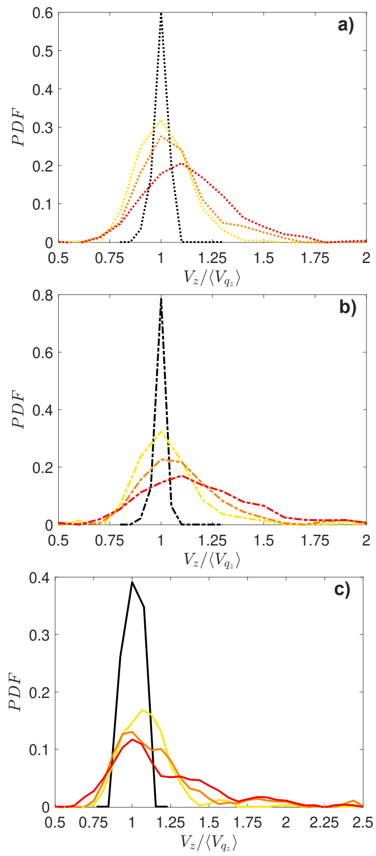

Figure 6. Probability density function (PDF) of the ratio of the measured mean descent velocity for disks falling in background turbulence (V_z) to the measured mean descent velocity of the disks in quiescent flow ($\langle V_{q_z}\rangle$). The colours of the PDF stand for different waiting times: yellow for $dt = 20$, orange for $dt = 10$ and red for $dt = 2$. a) Disk $\sharp 1$, b) Disk $\sharp 2$ and c) Disk $\sharp 3$.

tails of the red lines in figure 6 become wider towards the slower side of the velocity range.

Figure 7 shows a sample trajectory of disk $\sharp 1$ that contains a trajectory section with very low velocity magnitude during a significant period of time (shaded in green). In fact, the descent velocity during this interval of time never exceeds half of the maximum descent velocity in quiescent flow, and this is maintained for a duration corresponding to two particle oscillatory periods in quiescent flow. From the evolution of the speed and the descent velocity (figure 7 b) and c) respectively) one can observe that this event occurs in between two sections of 'standard' descend and therefore is completely induced by turbulence. This highlights the influence of background turbulence in the local dynamics of the disk and shows that certain particle-turbulence configurations can lead to a severe reduction of the descent velocity and total speed for long durations. These trajectories, with 'slow' and 'fast' events contained within a single descent illustrate the complexity of the disk trajectories when background turbulence is introduced.

Conclusion

The free-fall motion of thin disks released in homogeneous turbulence was investigated experimentally. We used a stereoscopic vision technique to extract 3-D trajectory in-

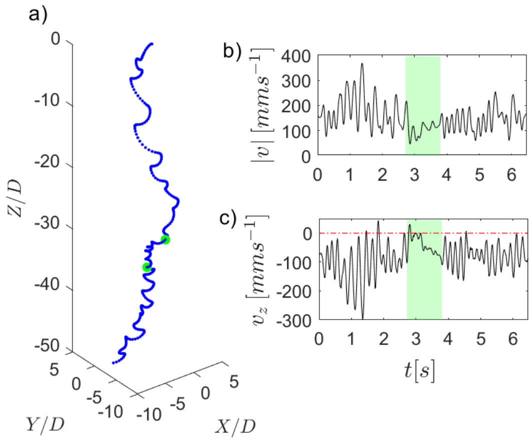

Figure 7. 'Slow' event during the descend of disk ♯1 under turbulence effects released after a waiting time $dt = 2$. a) Reconstructed 3D trajectory with the dispersion normalized with the disk diameter, green dots show the start and end of the 'slow' subsection. b-c) Time evolution of the particle speed and particle descent velocity, the green shaded region showing the 'slow' subsection.

formation on the particle falling style and mean descent velocity.

Regarding the falling style, we showed that disks can describe very long gliding sections during the fluttering motion and we hypothesize that this is caused by large turbulent structures moving locally with the disk. We also observed that the long gliding sections are associated with higher particle nutation angles, and therefore this type of motion enhances descent velocity and particle dispersion. Similarly, we observed that disks under strong turbulence effects might describe characteristic features of other falling styles than the ones associated with the regime where they lie (in the $Re - I^*$ domain for quiescent flow). More precisely, disks are reported to describe tumbling motions in between sections of 'standard' fluttering. In contrast, in some realizations the particle mean descent velocity is severely reduced and we observed sections of the trajectory where the particle hardly descents while it keeps describing fluttering-type oscillations.

On the other hand, we observed an increase in mean descent velocity in all cases investigated. The increase in the mean descent velocity highlights the severe differences between spherical and non-spherical particles since the cases investigated correspond to the velocity reduction region for spherical particles ($\langle V_z \rangle / u' > 1$). We believe that the physical mechanisms responsible of the change in the descent velocity of aspherical planar particles are different from the ones observed for spheres. In the case of small and heavy spherical particles the natural descent is nearly steady, whereas for finite-size inertial disks the trajectories exhibit severe velocity fluctuations with instants of zero velocity. Similarly, the descent of finite-size inertial disks is highly influenced by the orientation of the particle and this can be easily modified by turbulence structures specially near the zero velocity points. We also found that turbulence to quiescent descent velocity ratio is not the only parameter responsible for the velocity enhancement in disks because particles with different material properties show a different increase in velocity for similar velocity ratios. Thus, we hypothesize that this velocity ratio might not be the appropriate parameter to identify whether particles with strong secondary motions will experience an enhancement or reduction of the settling speed.

REFERENCES

Auguste, F., Magnaudet, J. & Fabre, D. 2013 Falling styles of disks. *J. Fluid Mech.* **719**, 388–405.

Bellani, G. & Variano, E. A. 2013 Homogeneity and isotropy in a laboratory turbulent flow. *Exp. Fluids* **55**, 1646–1666.

Byron, M., Einarsson, J., Gustavsson, K., Voth, G., Mehlig, B. & Variano, E. 2015 Shape-dependence of particle rotation in isotropic turbulence. *Phys. Fluids* **27**, 035101.

Carter, D., Petersen, A., Amili, O. & Coletti, F. 2016 Generating and controlling homogeneous air turbulence using random jet arrays. *Experiments in Fluids* **57**, 189.

Churst, M., Bouchet, G. & Dusek, J. 2013 Numerical simulation of the dynamics of freely falling discs. *Physics of Fluids* **25**, 044102.

Esteban, L. B., Shrimpton, J. S. & Ganapathisubramani, B. 2018 Edge effects on the fluttering characteristics of freely falling planar particles. *Physical Review Fluids* **3**, 064302.

Esteban, L. B., Shrimpton, J. S. & Ganapathisubramani, B. 2019 Study of the circularity effect on drag of disk-like particles. *International Journal Multiphase Flows* **110**, 189–197.

Field, S. B., Klaus, M., Moore, M. G. & Nori, F. 1977 Chaotic dynamics of falling disks. *Nature* **388**, 252–254.

Good, G. H., Gerashchenko, S. & Warhaft, Z. 2012 Intermittency and inertial particle entrainment at a turbulent interface: the effect of the large-scale eddies. *J. Fluid Mech.* **694**, 371—398.

Good, G. H., Ireland, P. J., Bewley, G. P., Bodenschatz, E., Collins, L. R. & Warhaft, Z. 2014 Settling regimes of inertial particles in isotropic turbulence. *J. Fluid Mech.* **759** (R3), 1–12.

Heisinger, L., Newton, P. & Kanso, E. 2014 Coins falling in water. *J. Fluid Mech.* **714**, 243–253.

Lee, C., Su, Z., Zhong, H., Chen, S., Zhou, M. & Wu., J. 2013 Experimental investigation of freely falling thin disks. part 2. transition of three-dimensional motion from zigzag to spiral. *J. Fluid Mech.* **732**, 77–104.

Nielsen, P. 1993 Turbulence effects on the settling of suspended particles. *Journal of Sedimentary Research* **63(5)**, 835—-838.

Variano, E. A. & Cowen, E. A. 2008 A random-jet-stirred turbulence tank. *J. Fluid Mech* **604**, 1–32.

Willmarth, W. W., Hawk, N. E. & Harvey, R. L. 1964 Steady and unsteady motions and wakes of freely falling disks. *Phys. Fluids* **7**, 197–208.

Zhong, H., Chen, S. & Lee, C. 2011 Experimental study of freely falling thin disks: transition from planar zigzag to spiral. *Phys Fluids* **23**, 011–702.

Zhong, H., Lee, C., Su, Z., Chen, S., Zhou, M. & Wu., J. 2013 Experimental investigation of freely falling thin disks. part 1. the flow structures and reynolds number effects on the zigzag motion. *J. Fluid Mech.* **716**, 228–250.